

Isoscaling in Light-Ion Induced Reactions and its Statistical Interpretation

A.S. Botvina,⁽¹⁾[a] O.V. Lozhkin,⁽²⁾ and W. Trautmann⁽¹⁾

⁽¹⁾*Gesellschaft für Schwerionenforschung, D-64291 Darmstadt, Germany*

⁽²⁾*V.G. Khlopin Radium Institute, 197002 St. Petersburg, Russia*

Isotopic effects observed in fragmentation reactions induced by protons, deuterons, and α particles of incident energies between 660 MeV and 15.3 GeV on ^{112}Sn and ^{124}Sn targets are discussed. The exponential scaling of the yield ratios with the third component of the fragment isospin $t_3 = (N - Z)/2$ is observed in all reactions, with scaling parameters that depend on the incident energy. Breakup temperatures for these reactions are deduced from double ratios of isotopic yields and tested for their relation with the isoscaling parameters.

The quantum statistical (QSM) and the statistical multifragmentation (SMM) models are used for interpreting the results. The observed isoscaling can be understood as a consequence of a statistical origin of the emitted fragments in these reactions. The SMM analysis shows that the exponent describing the isoscaling behavior is proportional to the strength of the symmetry term of the fragment binding energy. Using this result, a symmetry-term coefficient $\gamma \approx 22.5$ MeV for fragments at breakup is deduced from the experimental data. This is close to the standard value and supports SMM assumptions for the breakup configuration. An alternative method of determining the symmetry-energy coefficient, by using isotope distribution widths, is also discussed.

PACS numbers: 25.70.Mn, 25.70.Pq, 25.40.Sc

I. INTRODUCTION

Isotopic effects in nuclear reactions are receiving increasing attention because of their relation with the symmetry energy in the nuclear equation of state whose density dependence is of high current interest, in particular also for astrophysical applications [1, 2, 3, 4]. In a series of recent papers, the scaling properties of cross sections for fragment production with respect to the isotopic composition of the emitting systems were investigated by Tsang et al. [5, 6, 7]. The studied reactions include symmetric heavy-ion reactions at intermediate energy leading to multifragment-emissions as well as asymmetric reactions induced by α particles and ^{16}O projectiles at low to intermediate energies with fragment emission from excited heavy residues. The common behavior observed for these reactions, termed isoscaling, concerns the production ratios R_{21} for fragments with neutron number N and proton number Z in reactions with different isospin asymmetry. It is constituted by their exponential dependence on N and Z according to

$$R_{21}(N, Z) = Y_2(N, Z)/Y_1(N, Z) = C \cdot \exp(N \cdot \alpha + Z \cdot \beta) \quad (1)$$

with three parameters C , α and β . Here Y_2 and Y_1 denote the yields from the more neutron rich and the more neutron poor reaction system, respectively.

In some of the reactions, the parameters α and β have the tendency to be quite similar in absolute magnitude but of opposite sign. For multifragmentation following central collisions of $^{124}\text{Sn} + ^{124}\text{Sn}$ and $^{112}\text{Sn} + ^{112}\text{Sn}$ at 50 MeV per nucleon, $\alpha = 0.37$ and $\beta = -0.40$ was obtained from fits to the fragment yield ratios in the mass range $1 \leq A \leq 18$ [5]. These parameters suggest an approximate scaling with the third component of the isospin

$t_3 = (N - Z)/2$ of the form

$$R_{21}(N, Z) = C \cdot \exp((N - Z) \cdot \alpha) \cdot \exp(Z \cdot (\alpha + \beta)) \\ \approx C \cdot \exp(t_3 \cdot 2\alpha), \quad (2)$$

which follows from Eq. (1) since $\beta \approx -\alpha$.

The isotopic scaling of this latter kind has first been reported for reactions of protons of 660 MeV energy incident on targets of $^{112,124}\text{Sn}$ [8, 9] and subsequently also for other reactions with proton and deuteron projectiles in the relativistic regime of bombarding energies [10]. With the notation chosen in these early papers,

$$R_{12}(N, Z) = Y_1(N, Z)/Y_2(N, Z) = C \cdot \exp(-t_3 \cdot \beta_{t3}), \quad (3)$$

parameter values in the range $\beta_{t3} \approx 0.7$ were obtained for the reactions with p(6.7 GeV) and d(3.1 GeV) projectiles [11]. This is rather close to twice the value of α for the symmetric Sn + Sn reactions [5] and, according to Eq. (2), suggests a very similar scaling behavior for fragmentation reactions induced by relativistic light ions.

In this paper, we will discuss the isotopic effects observed by Bogatin et al. for reactions induced by protons, deuterons, and α particles of incident energies between 660 MeV and 15.3 GeV on $^{112,124}\text{Sn}$ targets [8, 9, 10, 12]. Particular emphasis will be given to their scaling properties, with the aim to incorporate the light-ion induced fragmentation into the set of reactions investigated by Tsang et al. [5]. A complete set of references to these data and a statistical analysis performed with the quantum statistical model (QSM) of Hahn and Stöcker [13] can be found in Ref. [14].

We will, furthermore, present isotopic temperatures derived from double ratios of helium and lithium isotopes for these reactions and compare their dependence

on the incident energy with that of the scaling parameters. Temperature measurements, in principle, also permit a test whether the reaction scenario, and specifically the temperature as an important parameter characterizing it, are indeed independent of the isotopic composition of the system as commonly assumed. For isotope temperatures, however, this property is already implied if isoscaling holds. It is a consequence of Eq. (1) according to which the double yield ratios from which isotope temperatures are derived are identical for the pair of reactions. The observations of approximately identical isotope temperatures in the $^{112}\text{Sn} + ^{112}\text{Sn}$ and $^{124}\text{Sn} + ^{124}\text{Sn}$ reactions at 50 MeV per nucleon [15], as well as for the present reactions, are therefore part of the more general phenomenon of isoscaling.

It has been shown that in both, light-ion induced collisions and peripheral heavy-ion collisions at high energy, the fragment production and observed isotopic effects can be explained in the framework of a hybrid approach consisting of a dynamical initial stage and a subsequent statistical breakup of a highly excited residual at low density [16, 17, 18, 19]. With the aim to identify reasons for the isotopic scaling in the present case, an analysis with the statistical multifragmentation model (SMM, Ref. [16]) was carried out. It will be demonstrated that isotopic scaling arises naturally in a statistical fragmentation mechanism. The isoscaling parameter α deduced for hot primary fragments is, furthermore, found to be directly proportional to the symmetry part of the binding energy of the fragments when they are formed at low density. To the extent that the modification of this parameter during secondary deexcitation remains small this opens the possibility of testing components of the nuclear equation of state in fragmentation reactions.

II. EXPERIMENTAL DATA

The experimental data are taken from the literature [8, 9, 10, 12]. They were obtained in the JINR laboratories in Dubna with beams of protons of 660 MeV, 1.0 and 6.7 GeV, of deuterons with 3.1 GeV, and of α particles with 15.3 GeV incident energy. Isotopically resolved cross sections of light fragments were measured with semiconductor telescopes placed at $\theta_{lab} = 90^\circ$ and with thin internal targets made from enriched ^{112}Sn ($\approx 81\%$) and ^{124}Sn ($\approx 96\%$). From the yields, integrated over energy intervals specified in Refs. [8, 10], ratios R_{12} for the production of a particular fragment in the reactions with the two Sn isotopes were determined. It is convenient to introduce a reduced isotopic effect for a fragment species X by normalizing with respect to the ratio observed for ^6Li , i.e. $R_{12}(X)/R_{12}(^6\text{Li})$. Uncertainties of the absolute normalizations of the data sets measured with the two targets are thus eliminated.

The reduced isotopic effects measured for the five pairs of reactions are shown in Fig. 1. The cross section ratios for the most neutron poor and the most neutron rich

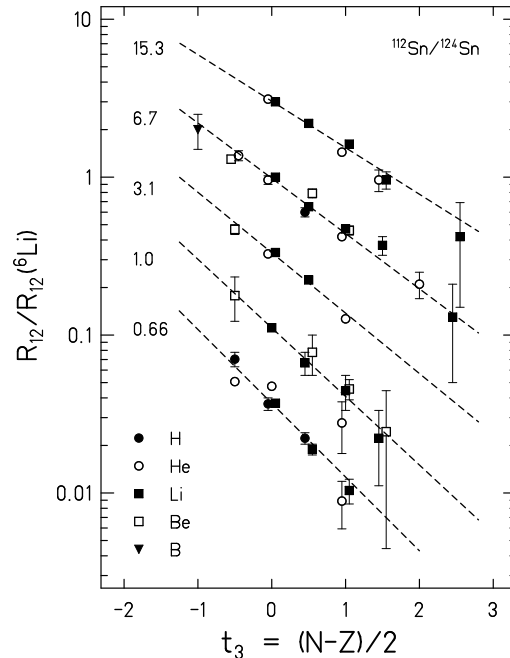


FIG. 1: Isotopic effect R_{12} , normalized with respect to $R_{12}(^6\text{Li})$, versus the third component of the fragment isospin t_3 . The five reactions are offset from each other by multiple factors of three and are labelled with the total projectile energy, given in units of GeV. H, He, Li, Be, and B fragments are distinguished by different data symbols as indicated. The lines are the results of exponential fits according to Eq. (3). Some of the data symbols are slightly displaced horizontally for reasons of clarity.

TABLE I: Parameters obtained from fitting the measured isotopic yield ratios with the scaling functions given in Eqs. (1) and (3). The second column gives the range of fragment Z over which the data sets extend.

Projectile	Z	β_{t_3}	α	β
p 0.66 GeV	1 - 3	1.08 ± 0.06	0.53 ± 0.04	-0.51 ± 0.05
p 1.00 GeV	2 - 4	1.00 ± 0.10	0.52 ± 0.04	-0.65 ± 0.05
d 3.10 GeV	2 - 4	0.88 ± 0.04	0.43 ± 0.03	-0.45 ± 0.04
p 6.70 GeV	1 - 5	0.81 ± 0.02	0.39 ± 0.01	-0.43 ± 0.02
α 15.3 GeV	2 - 3	0.68 ± 0.02	0.34 ± 0.01	-0.32 ± 0.03

fragments differ by about one order of magnitude in all cases except for the d(3.1 GeV) reaction for which only a narrow range of isospin is covered by the detected products. A nearly perfect exponential dependence on the third component t_3 of the fragment isospin is observed, with slope parameters β_{t_3} (Eq. (3)) that decrease gradually from 1.08 to 0.68 as the projectile energy increases (Table I). This variation of the isotopic effect with the incident energy has been noted in Ref. [14] and tentatively ascribed to a gradual rise of the temperatures of the emitting systems.

Two-parameter fits according to Eq. (1) were also performed, with results that are listed in Table I. The mono-

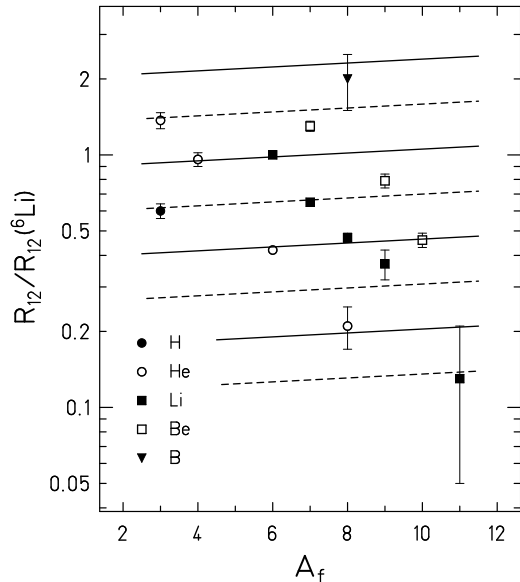


FIG. 2: Isotopic effect R_{12} , normalized with respect to $R_{12}({}^6\text{Li})$, versus the mass number A_f of the detected fragment for the reactions of protons with ${}^{112,124}\text{Sn}$ at 6.7 GeV. H, He, Li, Be, and B fragments are distinguished by different data symbols as indicated. The result of a three-parameter fit to the data according to Eq. (4) is represented by the lines of constant integer (full lines) and half-integer (dashed) isospin.

tonic trend exhibited by the parameter α as a function of the incident energy reflects that of β_{t_3} . It apparently extends to much lower energies, as evident from the value $\alpha = 0.60$ reported for the $\alpha(200 \text{ MeV})$ reaction in Ref. [5]. The dependence on Z is not equally well established for all reactions since only a limited range of elements has been covered in some cases. There is, however, a tendency of the absolute value of β being larger than α . For protons of 6.7 GeV, this is illustrated in Fig. 2 with the results from yet another parameterization in terms of A and t_3 ,

$$R_{12}(A, t_3) = C \cdot \exp(A \cdot \alpha_A + t_3 \cdot \beta'_{t_3}). \quad (4)$$

The logarithmic slope of the cross section ratios for given t_3 as a function of A , by its definition equal to half the difference between $|\beta|$ and α , is finite with a value $\alpha_A = (1.8 \pm 1.1) \cdot 10^{-2}$. Weighted over the five reactions $|\beta|$ is found to be larger than α by $8\% \pm 4\%$.

III. INITIAL DYNAMICAL STAGE

For the simulation of the initial stage of the collision the intranuclear cascade (INC) model developed in Dubna was used [20, 21]. The INC describes the process of the hadron-nucleon collisions inside the target nucleus. High energy products of these interactions are allowed to escape while low energy products are assumed to be trapped by the nuclear potential of the target system.

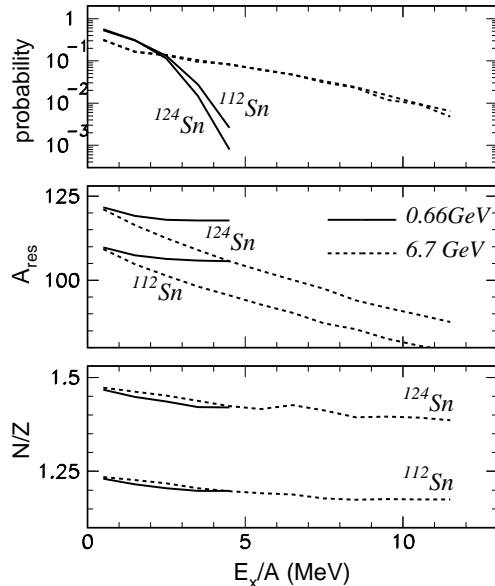


FIG. 3: Production probability of residual nuclei after the intranuclear cascade (top), their mean mass numbers A_{res} (middle), and their mean neutron-to-proton ratio N/Z (bottom) as a function of their excitation energies for collisions of protons with ${}^{112}\text{Sn}$ and ${}^{124}\text{Sn}$ targets at 660 MeV (solid lines) and 6.7 GeV (dashed lines).

At the end of the cascade, a residue with a certain mass, charge and excitation energy remains which then can be used as input for the statistical description of the fragment production.

For $p + {}^{112,124}\text{Sn}$ reactions, the obtained correlations between the mass number and the N/Z ratio of the residues with their excitation energy is shown in Fig. 3. The masses decrease with increasing excitation energy, a behavior that is well known [16, 21, 22, 23], but the rate is considerably lower for the lower proton energy. The N/Z ratio also decreases gradually for both targets with an apparently universal rate that does not depend much on the projectile energy nor on the neutron content of the target. As a consequence, the difference $\Delta(N/Z)$ on which the isotopic effect depends linearly in first order [3, 9] remains approximately constant. The calculated cross sections show that the covered range of excitation energies depends strongly on the proton energy.

It has been noticed repeatedly that the excitation energies obtained from first-stage reaction models are larger than needed to describe the observed fragment production with statistical multifragmentation models [18, 24, 25, 26, 27]. This effect has been interpreted as evidence for expansion and additional preequilibrium emission during an intermediate stage between the cascade termination and the fragment formation, not accounted for in the two-stage description. It leads to an uncertainty for the input parameters of the statistical calculations which has to be considered in their use and interpretation.

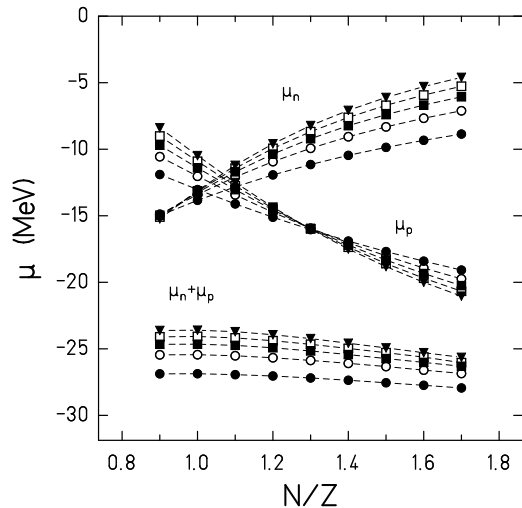


FIG. 4: Results of QSM calculations for neutron and proton chemical potentials μ_n and μ_p of systems with different densities ρ and N/Z ratios. The temperature is $T = 6$ MeV; the density increases from $\rho/\rho_0 = 0.1$ (dots) to 0.5 (triangles) in steps of 0.1 where ρ_0 is the normal nuclear density.

IV. CHEMICAL EQUILIBRIUM

Isotopic effects and isotope yield ratios confront us with the question of chemical equilibrium in the system. Here, the grand-canonical quantum-statistical models (QSM) are useful for extracting relative isotopic abundances that correspond to the thermodynamical limit. The model of Hahn and Stöcker [13], chosen in the present case, assumes thermal and chemical equilibrium at the breakup point where the fragmenting system is characterized by a density ρ , temperature T , and by its overall N/Z ratio. The model respects fermion and boson statistics which, however, is not crucial at high temperature. It does not take into account the finite size of the nuclear systems nor the Coulomb interaction between fragments but follows the sequential decay of excited fragments according to tabulated branching ratios. It has already been shown that the t_3 scaling (Eq. (3)) exhibited by the $p(6.7 \text{ GeV}) + {}^{112,124}\text{Sn}$ reactions is well reproduced by the QSM if appropriate parameters are chosen [14]. Even if $\Delta(N/Z)$ is fixed, e.g. with the aid of the INC model, a continuous set of pairs of $T - \rho$ parameters can be found that all permit equally good descriptions of the data. By varying either the temperature or the density the observed variation of the scaling parameter with incident energy can be followed.

In the grand-canonical approximation, the scaling parameters α and β (Eq. (1)) are equal to the difference of the chemical potentials for neutrons and protons in the two systems, $\alpha = \Delta\mu_n/T$ and $\beta = \Delta\mu_p/T$, provided a common temperature T for both systems exists [5, 28]. The observation of t_3 scaling, consequently, implies that these differences are of different sign and about equal

TABLE II: Apparent temperatures deduced from He and Li isotopic yield ratios, as indicated in column 2, for reactions with the ${}^{112}\text{Sn}$ and ${}^{124}\text{Sn}$ targets.

Projectile	isotopes	${}^{112}\text{Sn}$	${}^{124}\text{Sn}$
p 0.66 GeV	${}^{3,4}\text{He}$, ${}^{6,7}\text{Li}$	3.8 ± 0.1 MeV	4.6 ± 0.1 MeV
p 1.00 GeV	${}^{4,6}\text{He}$, ${}^{6,8}\text{Li}$	2.2 ± 0.2 MeV	2.6 ± 0.2 MeV
d 3.10 GeV	"	2.7 ± 0.2 MeV	3.1 ± 0.2 MeV
p 6.70 GeV	"	2.9 ± 0.2 MeV	2.9 ± 0.2 MeV
α 15.3 GeV	"	3.3 ± 0.2 MeV	3.5 ± 0.2 MeV
p 6.70 GeV	${}^{6,8}\text{He}$, ${}^{6,8}\text{Li}$	4.6 ± 0.4 MeV	4.7 ± 0.3 MeV
α 15.3 GeV	"	4.3 ± 0.5 MeV	3.8 ± 0.3 MeV

magnitude, or that the sum of μ_n and μ_p is invariant with the N/Z ratio of the system. This is illustrated in Fig. 4 in which the chemical potentials extracted from the model calculations are given as a function of N/Z . The chosen parameters are $T = 6$ MeV and ρ/ρ_0 from 0.1 to 0.5 in steps of 0.1 (the $p(6.7 \text{ GeV})$ data, e.g., are reproduced with $T = 6$ MeV and $\rho/\rho_0 = 0.1$ [14]). The sum $\mu_n + \mu_p$ is approximately independent of N/Z , with a very small tendency of μ_p to change more rapidly than μ_n .

For the Sn isotopes with $N/Z = 1.24$ and 1.48 and for a breakup density $\rho/\rho_0 = 0.3$ the calculated differences of the chemical potentials are $\Delta\mu_n = 2.3$ MeV and $\Delta\mu_p = -2.9$ MeV. From these values coefficients $\alpha = 0.38$ and $\beta = -0.48$ are obtained which are not far from the experimental observation in central Sn + Sn collisions [5] and in some of the present reactions. A more stringent model test will have to include a comparison with fragment yields and an accurate estimation of the temperature. However, as also shown in Ref. [14], the chemical equilibrium hypothesis is quite adequate for the description of isotopic phenomena in these reactions even though the heavy fragments or residues in the final channels are not explicitly taken into account. These degrees of freedom will be included in the SMM analysis presented in Section VI.

V. TEMPERATURES

The reported cross sections for helium and lithium isotopes were used to construct temperature observables from double-isotope ratios [28] for the present set of reactions. The production of ${}^{3,4}\text{He}$ and of ${}^{6,7}\text{Li}$ has been measured for incident protons of 660 MeV, and the frequently used T_{HeLi} temperature [23] can be determined for this particular case. Cross sections for the production of ${}^3\text{He}$ are not reported for the reactions at higher energies, so that T_{HeLi} cannot be used to follow the evolution of the breakup temperature with incident energy.

A common temperature observable for four out of the set of five reactions can be obtained from the ${}^4\text{He}/{}^6\text{He}$ and ${}^6\text{Li}/{}^8\text{Li}$ yield ratios, and in two cases ${}^6\text{He}$ and ${}^8\text{He}$ yields are available which can also be combined with the

lithium ratios ${}^6\text{Li}/{}^8\text{Li}$. The corresponding expressions are

$$T_{\text{HeLi},0} = 13.3 \text{ MeV} / \ln(2.2 \frac{Y_{{}^6\text{Li}}/Y_{{}^7\text{Li}}}{Y_{{}^3\text{He}}/Y_{{}^4\text{He}}}); \quad (5)$$

$$T_{\text{He46/Li68},0} = -8.3 \text{ MeV} / \ln(1.4 \frac{Y_{{}^6\text{Li}}/Y_{{}^8\text{Li}}}{Y_{{}^4\text{He}}/Y_{{}^6\text{He}}}); \quad (6)$$

$$T_{\text{He68/Li68},0} = 7.2 \text{ MeV} / \ln(1.7 \frac{Y_{{}^6\text{Li}}/Y_{{}^8\text{Li}}}{Y_{{}^6\text{He}}/Y_{{}^8\text{He}}}). \quad (7)$$

The two latter isotopic thermometers do not fulfill the requirement that the double difference of the binding energies of the four isotopes, the prefactor in Eqs. (5) - (7), should be large compared to the anticipated temperatures [23, 29]. They may thus be more strongly influenced by sequential decays. In particular, the contributions from residue evaporation to the inclusive yields of ${}^4\text{He}$ will have a large effect on $T_{\text{He46/Li68}}$. The true breakup temperature is likely to be underestimated by this observable but its trend with incident energy may be preserved. Therefore, at this stage, no attempt has been made to derive corrections, and the so-called apparent temperatures, labelled with the subscript 0 in the above expressions, are presented in Table II and Fig. 5. The differences of the energy intervals of the fragment detection [8, 10] and the systematic errors associated with the isotope identification [12] are taken into account.

The deduced values of $T_{\text{HeLi},0}$ and $T_{\text{He68/Li68},0}$ of about 4 to 5 MeV are in the range typical for reaction processes near the onset of multi-fragment emissions [23, 29, 30, 31]. The values obtained for $T_{\text{He46/Li68},0}$ are lower by 1 MeV or more, as expected. Most of the temperatures, within errors, are about equal for the corresponding pairs of reactions. Larger differences, as e.g. of $T_{\text{HeLi},0}$ for protons of 660 MeV, reflect similarly prominent deviations from isoscaling for some of the isotopes involved (cf. Fig. 1).

The trend with incident energy exhibited by $T_{\text{He46/Li68},0}$ is found to follow very closely that of the inverse of the scaling parameters α and β_{t3} (Fig. 5). This suggests that the gradual flattening of the slopes of the isoscaling curves, as the projectile energy increases, is indeed caused by a rising mean temperature. A variation of isotopic observables associated with a temperature change has recently been reported for the fragmentation of ${}^{28}\text{Si}$ projectiles in collisions with ${}^{112,124}\text{Sn}$ targets at 30 and 50 MeV per nucleon [32].

VI. SMM INTERPRETATION

The statistical multifragmentation model (SMM) is based upon the assumption of statistical equilibrium at a low-density freeze-out stage [16]. All breakup channels (partitions) composed of nucleons and excited fragments

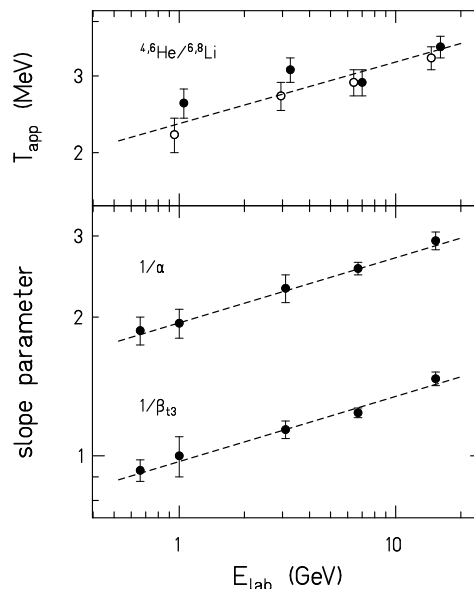


FIG. 5: Apparent isotope temperature T_{app} deduced from ${}^4,{}^6\text{He}$ and ${}^6,{}^8\text{Li}$ yield ratios (top) and the inverse isoscaling parameters (bottom) $1/\alpha$ (Eq. (1)) and $1/\beta_{t3}$ (Eq. (3)) as a function of the total projectile energy. The dashed lines represent the logarithmic rise of $1/\beta_{t3}$, multiplied by appropriate factors for comparison with the trends observed for $1/\alpha$ and T_{app} .

are considered and the conservation of mass, charge, momentum and energy is taken into account. The formation of a compound nucleus is included as one of the channels. In the microcanonical treatment the statistical weight of decay channel j is given by $W_j \propto \exp S_j$, where S_j is the entropy of the system in channel j which is a function of the excitation energy E_x , mass number A_s , charge Z_s and other parameters of the source. In the standard version of the model, the Coulomb interaction between the fragments is treated in the Wigner-Seitz approximation. Different breakup partitions are sampled according to their statistical weights uniformly in the phase space. After breakup, the fragments propagate independently in their mutual Coulomb field and undergo secondary decays. The deexcitation of the hot primary fragments proceeds via evaporation, fission, or Fermi-breakup [33].

A. Liquid-drop description of primary fragments

An important difference of the SMM from other statistical models, e.g. QSM [13] or the Berlin statistical multifragmentation model [34, 35], is the treatment of the hot fragments at the freeze-out density. In the SMM light fragments with mass number $A \leq 4$ are considered as stable particles ("nuclear gas") with masses and spins taken from the nuclear tables. Only translational degrees of freedom of these particles contribute to the entropy of the system. Fragments with $A > 4$ are treated as heated

nuclear liquid drops, and their individual free energies F_{AZ} are parameterized as a sum of the bulk, surface, Coulomb and symmetry energy contributions

$$F_{AZ} = F_{AZ}^B + F_{AZ}^S + E_{AZ}^C + E_{AZ}^{sym}. \quad (8)$$

The standard expressions [16] for these terms are: $F_{AZ}^B = (-W_0 - T^2/\epsilon_0)A$, where the parameter ϵ_0 is related to the level density, and $W_0 = 16$ MeV is the binding energy of infinite nuclear matter; $F_{AZ}^S = B_0 A^{2/3} (\frac{T_c^2 - T^2}{T_c^2 + T^2})^{5/4}$, where $B_0 = 18$ MeV is the surface coefficient, and $T_c = 18$ MeV is the critical temperature of infinite nuclear matter; $E_{AZ}^C = cZ^2/A^{1/3}$, where c is the Coulomb parameter obtained in the Wigner-Seitz approximation, $c = (3/5)(e^2/r_0)(1 - (\rho/\rho_0)^{1/3})$, with the charge unit e and $r_0 = 1.17$ fm; $E_{AZ}^{sym} = \gamma(A - 2Z)^2/A$, where $\gamma = 25$ MeV is the symmetry energy parameter.

These parameters are those of the Bethe-Weizsäcker formula and correspond to the assumption of isolated fragments with normal density in the freeze-out configuration, an assumption found to be quite successful in many applications. It is to be expected, however, that in a more realistic treatment primary fragments will have to be considered not only excited but also expanded and still subject to a residual nuclear interaction between them. These effects can be accounted for in the fragment free energies by changing the corresponding liquid-drop parameters, provided such modifications are also indicated by the experimental data. In the following, it will be shown that, for the symmetry energy, this information may be obtained from the isoscaling phenomenon.

B. Grand canonical approximation

In the grand canonical approximation, first developed in Ref. [36], the mean multiplicity of a fragment with mass number A and charge Z is given by

$$\langle N_{AZ} \rangle = g_{AZ} \frac{V_f}{\lambda_T^3} A^{3/2} \exp \left[-\frac{1}{T} (F_{AZ}(T, \rho) - \mu A - \nu Z) \right] \quad (9)$$

where g_{AZ} is the degeneracy factor of the fragment, λ_T is the nucleon thermal wavelength, V_f is the "free" volume, and μ and ν are the chemical potentials responsible for the mass and charge conservation in the system, respectively [16]. It follows immediately that, for two systems 1 and 2 with different total mass and charge but with the same temperature and density, the ratio of fragment yields produced in these systems is given by Eq. (1) with parameters $\alpha = (\mu_1 - \mu_2)/T$ and $\beta = ((\mu_1 - \mu_2) + (\nu_1 - \nu_2))/T$. Isoscaling arises very naturally in the SMM.

Calculated chemical potentials for systems with different mass and N/Z ratio as a function of the temperature are shown in Fig. 6. A freeze-out density $\rho/\rho_0 = 1/3$ has been chosen but, as apparent from the QSM calculations (Fig. 4), other densities lead to a similar behavior of

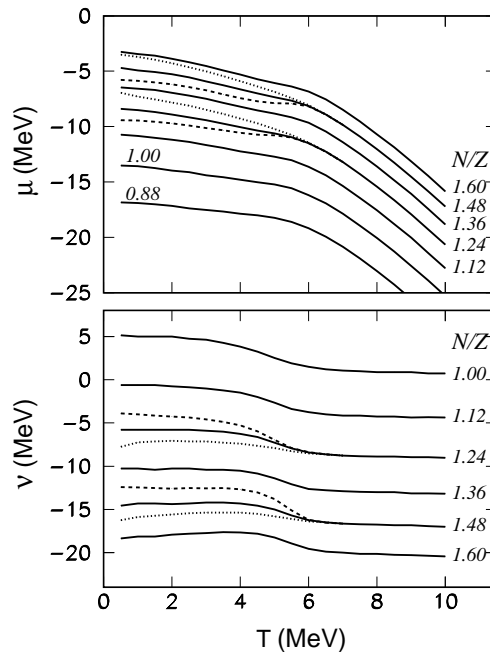


FIG. 6: Results of SMM calculations in the grand canonical approximation for the chemical potentials μ (top) and ν (bottom) as a function of the temperature of systems with different N/Z ratios as indicated and with sizes $Z = 50$ (solid lines), $Z = 100$ (dashed), and $Z = 25$ (dotted). The density is $\rho = \rho_0/3$.

the chemical potentials. Furthermore, corresponding to the excluded volume approximation [16], a fixed "free" volume $V_f = 2V_0$ (V_0 is the volume of the system at normal density) has been used instead of a multiplicity-dependent volume. For other parameters of the model their standard values were chosen, see e.g. Ref. [17].

The potential μ decreases with the temperature which has the simple physical meaning that the average size (mass number) of the produced fragments decreases. However, two regions with different rates of the change in fragment mass can be discerned. At low temperature, the rate is small, especially for large systems. Here the corresponding mass distribution is of the so-called "U-shape", with a compound-like fragment still dominating in the system. At temperatures near 5 to 6 MeV the rate increases rapidly. At this point, the "U-shape" disappears and the system disintegrates into many fragments with an approximately exponential mass distribution.

The behavior of the chemical potential ν is particularly interesting. As shown in Ref. [33], the average charge $\langle Z_A \rangle$ of fragments with mass A can be written as

$$\langle Z_A \rangle \simeq \frac{(4\gamma + \nu)A}{8\gamma + 2cA^{2/3}}. \quad (10)$$

The chemical potential ν is, therefore, directly connected with the isospin of the produced fragments. In grand-canonical models, as e.g. in the QSM [13], sometimes the

chemical potentials μ_n and μ_p , responsible for the conservation of the total numbers of neutrons and protons, are used. If expressed in terms of the SMM potentials, they are $\mu_n = \mu$ and $\mu_p = \mu + \nu$, with the consequence that not only μ_n but also μ_p will decrease with T ; the mean numbers of both, neutrons and protons, in the produced fragments decreases as their mass decreases. By using the potentials μ and ν the variations of the average mass and of the isotopic composition are separated.

The potential ν is nearly constant at both low and high temperature. These limits correspond to the isospin of fragments produced at the "liquid" and "gas" phases. There is a relatively fast transition between these limits at a temperature of 5 to 6 MeV, leading to a growing neutron content of light fragments as the "U-shape" disappears. This evolution of the fragment isospin has been confirmed by microcanonical calculations [37]. It is apparent from Fig. 6 that the effect is more pronounced for larger systems and that its relative magnitude depends weakly on the overall N/Z ratio.

For systems with different mass but with the same N/Z ratio, the chemical potentials differ only in the "U-shape" region at low temperatures. At high temperature, the chemical potentials coincide which leads to a total scaling of the fragment yields for systems of all sizes. This is equivalent to what is obtained by applying the grand canonical ensemble for the region of abundant multifragmentation. Examples of fragment charge distributions that are independent of the system size have been presented recently [38].

C. Chemical potentials

It is the difference of the chemical potentials of systems with different N/Z ratios that is directly connected with the isoscaling phenomenon. Results of calculations for the two tin isotopes are shown in Fig. 7. Despite of a considerable variation of the individual potentials, their differences $\Delta\mu = \mu_{112} - \mu_{124}$ and $\Delta\nu = \nu_{112} - \nu_{124}$ change only slightly as a function of the temperature. For the lower density $\rho/\rho_0 = 1/6$, an increased modulation is observed but, overall, the potential differences remain remarkably stable in the most important temperature region. This means that a variation of the scaling parameters β_{t3} or $\alpha = \Delta\mu/T$ is connected with a temperature change as suggested by the comparisons shown in Fig. 5.

Calculations were also performed with the Markov-chain version of the SMM with parameters identical to those used for the grand-canonical calculations. The Markov-chain model is a completely microcanonical approach which exactly conserves mass, charge, energy, and linear and angular momentum [37]. It was used to calculate the ratios of isotopes produced by the two different sources and the microcanonical temperature T_{micr} of the system, where T_{micr} is taken as the mean temperature of the generated partitions at a fixed excitation energy.

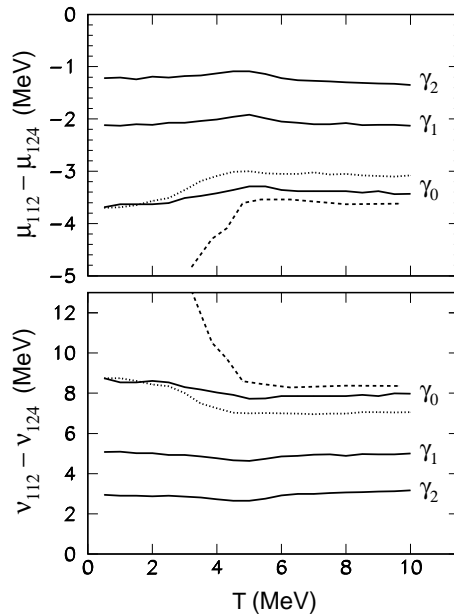


FIG. 7: Differences of the chemical potentials μ (top) and ν (bottom) for the ^{112}Sn and ^{124}Sn systems as a function of the temperature and for symmetry term coefficients $\gamma_0 = 25$ MeV, $\gamma_1 = 14.4$ MeV and $\gamma_2 = 8.3$ MeV. Solid and dotted lines represent grand canonical calculations for $\rho = \rho_0/3$ and $\rho = \rho_0/6$, respectively. The dashed lines are microcanonical Markov-chain calculations for $\rho = \rho_0/3$.

From these quantities effective potential differences $\Delta\mu$ and $\Delta\nu$ were determined according to

$$\Delta\mu = T_{\text{micr}} * \ln\left(\frac{Y_1(A, Z)Y_2(A+1, Z)}{Y_2(A, Z)Y_1(A+1, Z)}\right), \quad (11)$$

$$\Delta\nu = T_{\text{micr}} * \ln\left(\frac{Y_1(A, Z)Y_2(A, Z+1)}{Y_2(A, Z)Y_1(A, Z+1)}\right). \quad (12)$$

Here only light fragments with Z from 3 to 6 were used, similar to the experimental case. These potentials are very close to the grand-canonical results at temperatures $T > 5$ MeV which are of relevance for the production of fragments. The remaining small difference may arise from the need of using slightly different ensembles in the two types of calculations. At low temperatures the results diverge, indicating that here the exact conservation of mass, charge and energy is essential (cf. Fig. 5.6 in Ref. [16]). A small difference to the results reported in Ref. [6] exists insofar as the variations of $\Delta\mu_n$ and $\Delta\mu_p$ at high temperature, obtained there in the canonical approximation, are not reproduced by the present calculations. It may be a consequence of the constraint of the energy conservation, of another method of calculating chemical potentials, or of other differences of the used model versions. The grand-canonical QSM calculations predict negligible variations of the potential differences with temperature.

The symmetry term in the binding energy strongly influences the potential differences $\Delta\mu$ and $\Delta\nu$. This is illustrated in Fig. 7 with examples obtained for values $\gamma_1 = 14.4$ MeV and $\gamma_2 = 8.3$ MeV, both smaller than the standard value $\gamma_0 = 25$ MeV. The effect is significant and, in particular, larger than the variations associated with the choice of ensembles or with the choice of the density and, therefore, should be observable.

As the comparison shows, the grand-canonical approach is applicable only (i) if the average mass of the largest fragment of a partition is considerably less than the total size of the system, and (ii) if the extra energy necessary for the production of an additional fragment is small compared to the available thermal energy. However, because the difference of the chemical potentials is nearly constant in the full temperature range, the values obtained in the grand-canonical approximation at low temperatures may be extrapolated to high temperatures and applied in the multifragmentation region. In the low temperature limit $T \rightarrow 0$, analytical formulae for $\Delta\mu$ and $\Delta\nu$ can be derived. Here only channels including a compound-like nucleus with $A \approx A_0$ and $Z \approx Z_0$ will exist, where A_0 and Z_0 denote the mass and atomic number of the system. Mathematically, it is required that the numerator under the exponent in Eq. (9) approaches zero, i.e.

$$F_{A_0 Z_0}(T \rightarrow 0) = \mu A_0 + \nu Z_0, \quad (13)$$

which is equivalent to the thermodynamical potential of the compound nucleus being zero. From Eq. (10), with the same approximations, the potential

$$\nu \simeq \frac{Z_0}{A_0}(8\gamma + 2cA_0^{2/3}) - 4\gamma \quad (14)$$

can be obtained. Inserting this expression into Eq. (13) yields the chemical potential

$$\mu \simeq -W_0 + \frac{B_0}{A_0^{1/3}} - c\frac{Z_0^2}{A_0^{4/3}} + \gamma(1 - (\frac{2Z_0}{A_0})^2). \quad (15)$$

The terms small compared to the bulk terms can be safely disregarded (the errors are below 3% for the $^{112,124}\text{Sn}$ isotopes considered here). This leads to

$$\begin{aligned} \Delta\mu &= \mu_1 - \mu_2 \approx -4\gamma\left(\frac{Z_1^2}{A_1^2} - \frac{Z_2^2}{A_2^2}\right), \\ \Delta\nu &= \nu_1 - \nu_2 \approx 8\gamma\left(\frac{Z_1}{A_1} - \frac{Z_2}{A_2}\right), \end{aligned} \quad (16)$$

where Z_1, A_1 and Z_2, A_2 are the charges and mass numbers of the two systems. The potential differences depend essentially only on the coefficient γ of the symmetry term and on the isotopic compositions.

The values of the chemical potentials deduced in this limit are close to the separation energies of nucleons, apart from the difference in sign (see also Ref. [6]). For

example, the neutron separation energy s_n in the liquid-drop approximation is given by

$$s_n \approx W_0 - \gamma(1 - (\frac{2Z_0}{A_0})^2) - \frac{2B_0}{3A_0^{1/3}} + \frac{e^2 Z_0^2}{5r_0 A_0^{4/3}}. \quad (17)$$

The surface and Coulomb terms in this expression appear with different coefficients than in Eq. (15) but are, again, usually small in comparison to the dominating bulk (volume and symmetry) terms. As expected from the definitions of the chemical potential and the separation energy, this correspondence must be exact in the thermodynamical limit.

From Eqs. (16) another interesting relation can be deduced:

$$\Delta\mu \approx -\frac{\Delta\nu}{2}\left(\frac{Z_1}{A_1} + \frac{Z_2}{A_2}\right). \quad (18)$$

It implies $|\Delta\nu| > |2\Delta\mu|$ or, equivalently, $|\Delta\mu_p| > |\Delta\mu_n|$, for the usually considered systems with $A > 2Z$. Although the effects of secondary deexcitation are important (see below) this inequality is reflected by the observed scaling parameters. The magnitude of β exceeds that of α in all reactions discussed in Ref. [5] and, on average, also in the reactions presented here (Table I).

D. Fragment distribution widths

There is a simple physical explanation within the SMM why isoscaling should appear in finite systems. Charge distributions of fragments with fixed mass numbers A , as well as mass distributions for fixed Z , are approximately Gaussian with average values and variances which are connected with the temperature, the symmetry coefficient, and other parameters [36]. With a Gaussian distribution for an observable X (mass number or charge), $Y(X) \propto \exp(-(X - \langle X \rangle)^2 / 2\sigma^2)$, the ratio of this observable for two different systems is given by

$$\frac{Y_1(X)}{Y_2(X)} = \exp\left(-\frac{X^2}{2}\left(\frac{1}{\sigma_1^2} - \frac{1}{\sigma_2^2}\right) + X\left(\frac{X_1}{\sigma_1^2} - \frac{X_2}{\sigma_2^2}\right) + \text{const}\right), \quad (19)$$

where X_1, X_2 and σ_1, σ_2 are the mean values and variances for the two systems. The mean values depend on the total mass and charge of the systems, e.g. via the chemical potentials in the grand canonical approximation (Eq. (10)), while the variances depend mainly on the physical conditions reached, the temperature, the density and possibly other variables. For example, the charge variance $\sigma_Z \approx \sqrt{(AT/8\gamma)}$ obtained for fragments with a given mass number A in Ref. [36] is only a function of the temperature and of the symmetry term coefficient since the Coulomb contribution is very small. If these physical conditions are the same, i.e. $\sigma_1 = \sigma_2$, the exponential scaling for the ratio follows from Eq. (19). Furthermore, by using Eqs. (10) and (16) for $X = Z$, the approximate relation $\beta = \Delta\nu/T$ is again obtained, as in the usual grand-canonicals.

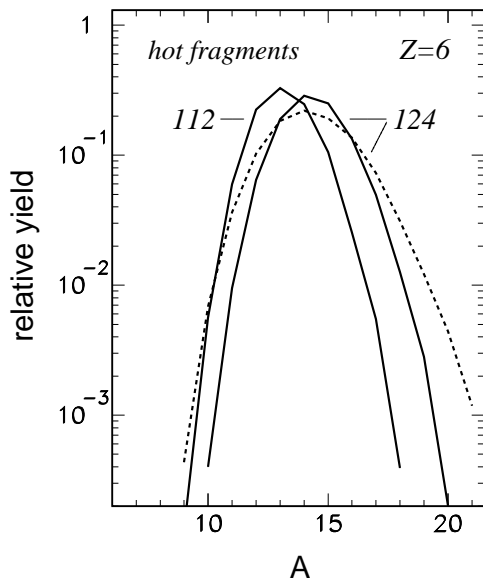


FIG. 8: Mass distributions of primary hot fragments with $Z = 6$ produced at freeze-out by ^{112}Sn and ^{124}Sn systems, as obtained from Markov-chain calculations for $E_x/A = 5$ MeV and $\rho = \rho_0/3$ (the corresponding microcanonical temperature is $T_{\text{micr}} \approx 5.3$ MeV). The symmetry coefficients $\gamma = 25$ MeV (solid lines) and $\gamma = 14.4$ MeV (dashed line) were used.

The Gaussian distributions obtained in the grand-canonical approximation are reproduced by the Markov-chain SMM calculations (Fig. 8). The mass distributions of fragments with $Z = 6$ emitted by ^{112}Sn and ^{124}Sn with $E_x/A = 5$ MeV are shifted with respect to each other because the N/Z ratios of the sources are different. Scaling will result, and the value of the scaling coefficient is determined by both, the shift, i.e. the difference in the mean masses, and the width of the distributions. The width, in turn, is influenced by the symmetry coefficient; with a reduced coefficient γ the mass distribution widens considerably (Fig. 8). Thus, if the temperature is known the symmetry coefficient can, in principle, be determined using the distributions.

The calculations indicate that the secondary deexcitation reduces both, the differences between the mean values of the distributions and the magnitude of the variances, thereby attaching a considerable uncertainty to this method. However, the sensitivity to the symmetry term coefficient survives the deexcitation stage. This is illustrated in Fig. 9 which shows the SMM predictions for the ratios of isotopic yields that are obtained for the same thermal source with different coefficients γ . The characteristic bell shape of the distributions reflects the quadratic term of Eq. (19) which dominates in this case when $\sigma_1 \neq \sigma_2$.

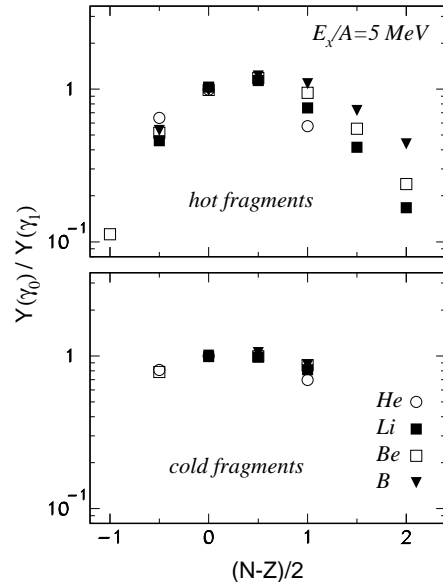


FIG. 9: Ratios of isotopic yields calculated for different symmetry coefficients $\gamma_0 = 25$ MeV and $\gamma_1 = 14.4$ MeV for the breakup of a ^{112}Sn source with $E_x/A = 5$ MeV at a density $\rho = \rho_0/3$. The top and bottom panels give the ratios for hot and cold fragments, respectively.

E. Secondary deexcitation of fragments

In the SMM the secondary deexcitation of large fragments with $A > 16$ is described with Weisskopf type evaporation and Bohr-Wheeler type fission models while the decay of small fragments is treated with a Fermi-breakup model [16, 33]. In this model all ground and nucleon-stable excited states of light fragments are taken into account and the population probabilities of these states are calculated according to the available phase space. The model thus simulates a simultaneous breakup microcanonically. This procedure is expected to reliably describe a decay that happens at short time scales after the freeze-out if the excitation energy of the primary fragments is high, of the order of 2-3 A MeV or higher.

The ratios of light element yields ($2 \leq Z \leq 5$) calculated with the Markov-chain SMM are shown in Fig. 10 for hot fragments produced at breakup and for cold fragments after the sequential decay. The exponential scaling with isospin is observed for both cases but with scaling coefficients that are systematically smaller for the final cold fragments (Table III). On more general grounds, it is expected that the scaling property is preserved because the excitation energies per nucleon are similar for all fragments, so that their relative nucleon content will decrease in a similar way. The secondary deexcitation has a trend, however, to populate the β -stable region which may reduce the shift between the mass distributions and also reduce their widths. A modification of the scaling coefficients is thus expected even though these two effects may partially compensate each other. In this respect,

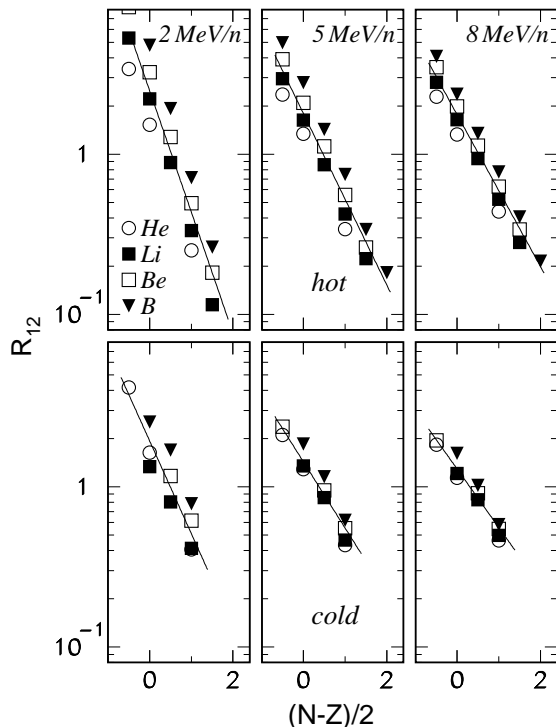


FIG. 10: Ratios of isotope yields produced at the breakup of ^{112}Sn and ^{124}Sn sources from Markov-chain SMM calculations for three excitation energies $E_x/A = 2, 5$ and 8 MeV and a density $\rho = \rho_0/3$. The top and bottom panels are for hot and cold fragments, respectively. The solid lines correspond to the logarithmic slope parameters β_{t3} given in Table III.

TABLE III: Parameters obtained from fitting the yield ratios of isotopes with $2 \leq Z \leq 5$ as calculated with the Markov-chain SMM for excitation energies $E_x/A = 2, 5$ and 8 MeV with the scaling functions given in Eqs. (1) and (3). Uncertainties are of the order of 0.01 to 0.02.

E_x/A (MeV)		β_{t3}	α	β
2	hot	1.74	0.93	-1.31
5	"	1.23	0.67	-0.91
8	"	1.09	0.57	-0.77
2	cold	1.33	0.69	-0.82
5	"	0.95	0.52	-0.63
8	"	0.84	0.45	-0.55

different isotopes can behave differently. The predicted reduction of the mass widths is typically 30% for boron isotopes, i.e. significant as expected, but is practically negligible for the lithium isotopes.

According to the calculations, the coefficients β_{t3} and α are reduced to, on average, 77% of their values by the secondary decay (Table III). The coefficient β is more strongly reduced to about 60% of its value at 2 AMeV and to about 70% at 8 AMeV. However, since the coefficients are decreasing with the energy, the absolute magnitude of this reduction decreases also. Moreover, additional

calculations showed that the secondary-decay effect decreases considerably if the coefficients themselves become smaller, e.g., a primary $\alpha \approx 0.46$ is reduced to ≈ 0.44 . In this respect, we confirm the conclusions of Ref. [6] regarding the minute variation of the α parameter, but provided that the value of the initial α is relatively small. The calculations of Ref. [6] were done for $E_x/A = 6$ MeV with several statistical models, including other versions of the SMM. In some of these calculations, the decay procedure is based on a sequential emission of particles from primary fragments, following the tabulated branching ratios and a Weisskopf scheme. This seems adequate for a later deexcitation stage with isolated fragments at relatively low excitation energy and without the influence of a common Coulomb field and without a residual nuclear interaction which can modify fragment properties including the branchings. The obtained modifications of the scaling parameter α do not exceed the order of 5% whereas β is reduced more strongly, similar to the present case.

The primary values of the scaling parameter $\alpha \approx 0.4$ to 0.45 reported in Ref. [6] for the $^{112,124}\text{Sn}$ systems are smaller than the corresponding values given in Table III. This, apparently, reflects significant differences between different versions and parameterizations of, in principle, the same model. They are of the same order as potential effects of the symmetry term that are to be studied. This emphasizes the need for exclusive analyses of experimental data which should constrain the model parameters. The two secondary deexcitation procedures should be considered as partly complementary, and the range of the differences of the obtained results may characterize the reliability of treating secondary decays with model calculations. These corrections are essential [39], but it will be important to reduce the uncertainties. Experimental methods, e.g. based on correlation techniques [40], may prove very useful for this purpose.

F. Interpretation of the data

The deduced relations will now be used for the interpretation of the experimental data. We will concentrate on the two reactions initiated by the projectiles with the highest energies, protons of 6.7 GeV and α particles of 15.3 GeV, for which the contributions from instantaneous breakups into multifragment channels should be enhanced in comparison to the other cases. The inclusive nature of the measurements, nevertheless, presents an inherent difficulty since a wide range of excitation energies is covered by the fragment emitting sources.

The $^{112,124}\text{Sn}$ targets used in these experiments were isotopically enriched to 81.7% and 96.6%, respectively [10, 12]. The effects of the impurities, known to be distributed approximately as the natural abundances of tin isotopes, have to be taken into account in a quantitative analysis. Corrections were estimated by assuming Gaussian mass distributions for the produced fragments,

centered around mean values that vary linearly with the mass number of the considered tin isotopes. It was found that, for the specific enrichments of the used targets and for scaling coefficients α in the range 0.3 to 0.6, the impurities cause a reduction of the measured α by 10% to 15%.

The analytical expressions for the differences of the chemical potentials, derived in the grand-canonical approximation (Eqs. (16)), depend only on γ and the isotopic composition of the sources. In the case of $\Delta\mu$, the difference of the squared Z/A values is required which is found to be the same within a few percent, independently of whether it is evaluated for the original targets $^{112,124}\text{Sn}$ or for the excited systems as predicted by the INC calculations (Fig. 3, Section III). For the original targets it amounts to $(Z_1/A_1)^2 - (Z_2/A_2)^2 = 0.0367$, leading to $\gamma = \Delta\mu/0.147$. To obtain an experimental value of $\Delta\mu = \alpha \cdot T$ (Section VI B), the mean values of the scaling coefficient α and of the isotope temperature $T_{\text{He68/Li68}}$ for the p(6.7 GeV) and $\alpha(15.3 \text{ GeV})$ reactions are used, after applying corrections. A measured $\langle\alpha\rangle = 0.365$ is obtained from Table I, corresponding to 0.417 for isotopically pure targets, and the effect of the secondary deexcitation is assumed to be 23%, as suggested by the Markov-chain calculations (Table III), thus leading to a primary $\alpha = 0.542$.

The predictions of the QSM [13] are used for the correction of the temperature. It does not significantly depend on the assumed density but it is large, as expected. The mean apparent temperature $T_{\text{He68/Li68},0} = 4.35 \text{ MeV}$ (Table II) corresponds to a breakup temperature $T = 6.2 \text{ MeV}$ in this model. The results obtained with these inputs are $\Delta\mu = 3.36 \text{ MeV}$ and $\gamma = 22.8 \text{ MeV}$, a symmetry coefficient slightly but not significantly smaller than the adopted standard value of 25 MeV.

For the interpretation of the isoscaling coefficient in the microcanonical limit the excitation energy needs to be specified. Exclusive data for hadron induced reactions on Au targets indicate that fragments will be emitted if energies exceeding $\approx 400 \text{ MeV}$, corresponding to $E_x/A \approx 2 \text{ MeV}$, are deposited by the projectile [41, 42]. Since the cross sections decrease and the fragment emission probabilities increase with excitation energy, a rather wide distribution results. For the π^- projectiles of 8 GeV/c studied by the ISiS collaboration this distribution extends from below 3 to above 8 MeV per nucleon with a weighted mean value of $E_x/A \approx 5 \text{ MeV}$ [41, 42]. A similar or, because of the lighter targets, a slightly higher value may be expected for the case of protons of 6.7 GeV on $^{112,124}\text{Sn}$. The INC calculations for this reaction, again weighted by the fragment production cross section, predict an average excitation energy $E_x/A = 6.2 \text{ MeV}$. With this interval 5.0 MeV to 6.2 MeV per nucleon for the excitation energy, and with the assumption that $\alpha \propto \gamma$ as in the grand-canonical approximation, values between $\gamma = 21.4 \text{ MeV}$ and 22.6 MeV are obtained from the comparison of the measured $\alpha = 0.39$ ($\alpha = 0.45$ for pure targets) with the predictions given in Table III for which

the standard value $\gamma = 25 \text{ MeV}$ was used. If $\langle E_x/A \rangle = 8 \text{ MeV}$ is considered as realistic for $\alpha(15.3 \text{ GeV})$ a similar symmetry coefficient $\gamma = 21.6 \text{ MeV}$ will result.

Towards the lower projectile energies, the isoscaling coefficient α increases up to 0.53, corresponding to 0.61 for pure targets, which is still lower than the SMM predictions for small excitation energies (Table III). With the INC result $\langle E_x/A \rangle = 2.7 \text{ MeV}$ for protons of 660 MeV, the interpolated prediction is $\alpha = 0.65$, and $\gamma = 23.3 \text{ MeV}$ is obtained from the comparison with the measured value. It thus seems that, for the reactions studied here, the deduced values of γ fall consistently into the range of 21 to about 23 MeV, with no significant dependence on the energy. In this respect, however, it has to be considered that the constraint of energy conservation in the microcanonical calculations may lead to unrealistically narrow widths of the isotope distributions at low excitation energies. This would cause an overprediction of the scaling coefficients and a deduced γ that is too low. This effect will bring γ even closer to the standard value for the reactions at lower incident energies which primarily proceed via the formation of excited compound nuclei.

VII. SUMMARY AND CONCLUSIONS

In the first part of this paper, the existence of isoscaling for reactions induced by relativistic light particles was demonstrated. The deduced exponents vary smoothly with the incident energy. Their trends, apparently, extend beyond the range studied here to low-energy projectiles as, e.g., α particles of 200 MeV for which isoscaling parameters were reported in Ref. [5]. The values obtained for protons of 6.7 GeV and α projectiles of 15.3 GeV are close to those for central $^{112,124}\text{Sn} + ^{112,124}\text{Sn}$ reactions at 50 MeV per nucleon given in the same reference. The observation of t_3 scaling was illustrated and discussed. As a function of the projectile energy, a very similar variation of the inverse scaling parameters and of the isotope temperature $T_{\text{He46/Li68}}$ was observed.

In the second part, a statistical formalism for the interpretation of the isoscaling phenomenon was developed. Analytical expressions were derived in the grand-canonical approximation and their validity and applicability illustrated. Results of calculations in the grand-canonical approximation and with the microcanonical Markov-chain version of the SMM were presented and the connection with the symmetry term of the fragment binding energy was established. It was found that the difference of the chemical potentials for the two isotopically different systems does not depend on the temperature. For the Markov-chain calculations, this conclusion is valid for temperatures $T \geq 5 \text{ MeV}$, the range of relevance for multifragment processes. The invariance of $\Delta\mu$ with temperature is consistent with the interpretation that the observed variation of the scaling parameters is caused by a change in temperature, as suggested by the

temperature measurement.

In the last part (Section VIF), an attempt was made to deduce values for the symmetry-energy coefficient γ from the experimental data. The analytical formulae derived in the grand-canonical limit of the SMM and the results of the microcanonical calculations were used and very similar values in the range $\gamma = 22.5 \pm 1$ MeV were obtained. Besides the scaling coefficient, experimental values for either the breakup temperature in the grand-canonical or for the excitation energy in the microcanonical approach were required. In the latter case, estimates obtained for similar reactions and from INC calculations were used.

We estimate the uncertainties of the methods, in particular the errors associated with the determinations of the breakup temperature or of the excitation energy for the microcanonical method, to be at least of the same order as the deviations of the results from the standard value $\gamma = 25$ MeV. The sequential decay corrections are substantial and, e.g., in the grand-canonical case are required twice, for the scaling coefficient and for the temperature. The present results, therefore, do not contradict the assumptions made in the statistical multifragmentation model in using standard liquid-drop parameters for describing the nascent fragments at the breakup stage.

A problem associated with the present data is the wide range of excitation energies over which an average is taken in the inclusive measurements. Smaller variations

may be smeared out. For these reasons, the presented analysis is primarily intended to serve as an example of how to extract the symmetry-energy coefficient γ from the experimental data. It is, nevertheless, of interest that the obtained result for fragmentation reactions induced by relativistic light projectiles has a tendency to be smaller than the conventional value of 25 MeV. A reduction with increasing energy may even be suggested by the microcanonical analysis. Provided it can be substantiated by other data and analyses, this would indicate that the symmetry part of the fragment binding energy is slightly weaker than that of isolated nuclei. Fragments, as they are formed at breakup, may have a lower than normal density. Such effects may be enhanced as the energy deposited in the fragmenting system is increased. Therefore, exclusive studies with possibly heavier projectiles will be required to more clearly identify potential variations of the symmetry energy with the reaction parameters.

Acknowledgments

Stimulating discussions with L. Andronenko, M. Andronenko, S. DasGupta, W.G. Lynch, I.N. Mishustin, M.B. Tsang and with the ALADIN group are acknowledged. One of the authors (A.S.B.) would like to thank the GSI for warm hospitality and support.

-
- [a] On leave from Institute for Nuclear Research, 117312 Moscow, Russia
- [1] H. Müller and B.D. Serot, *Phys. Rev. C* 52, 2072 (1995)
- [2] B.-A. Li, C.M. Ko, and W. Bauer, *Int. J. Mod. Phys. E* 7 147 (1998)
- [3] W.P. Tan, B.-A. Li, R. Donangelo, C.K. Gelbke, M.-J. van Goethem, X.D. Liu, W.G. Lynch, S. Souza, M.B. Tsang, G. Verde, A. Wagner, and H.S. Xu, *Phys. Rev. C* 64, 051901 (2001)
- [4] see also 'Isospin Physics in Heavy-ion Collisions at Intermediate Energies', edited by Bao-An Li and W.Udo Schröder, ISBN 1-56072-888-4, Nova Science Publ. Inc., New York (2001)
- [5] M.B. Tsang, W.A. Friedman, C.K. Gelbke, W.G. Lynch, G. Verde, and H.S. Xu, *Phys. Rev. Lett.* 86, 5023 (2001)
- [6] M.B. Tsang, C.K. Gelbke, X.D. Liu, W.G. Lynch, W.P. Tan, G. Verde, H.S. Xu, W.A. Friedman, R. Donangelo, S.R. Souza, C.B. Das, S. DasGupta, and D. Zhabinsky, *Phys. Rev. C* 64, 054615 (2001)
- [7] M.B. Tsang, W.A. Friedman, C.K. Gelbke, W.G. Lynch, G. Verde, and H.S. Xu, *Phys. Rev. C* 64, 041603 (2001)
- [8] V.I. Bogatin, V.K. Bondarev, V.F. Litvin, O.V. Lozhkin, N.A. Perfilov, Yu. P. Yakovlev, and V.P. Bochyn, *Yad. Fiz.* 19, 32 (1974) [*Sov. J. Nucl. Phys.* 19, 16 (1974)]
- [9] V.I. Bogatin, V.F. Litvin, O.V. Lozhkin, N.A. Perfilov, and Yu.P. Yakovlev, *Nucl. Phys. A* 260, 446 (1976)
- [10] V.I. Bogatin, E.A. Ganza, O.V. Lozhkin, Yu.A. Murin, V.S. Oplavin, N.A. Perfilov, and Yu. P. Yakovlev, *Yad. Fiz.* 31, 845 (1980) [*Sov. J. Nucl. Phys.* 31, 436 (1980)]; 34, 104 (1981) [34, 59 (1981)]
- [11] to avoid confusion with the notation of [5] the parameter β used in [8, 9, 10] is here represented by β_{t3}
- [12] V.I. Bogatin, E.A. Ganza, O.V. Lozhkin, Yu.A. Murin, V.S. Oplavin, N.A. Perfilov, and Yu. P. Yakovlev, *Yad. Fiz.* 36, 33 (1982) [*Sov. J. Nucl. Phys.* 36, 19 (1982)]
- [13] D. Hahn and H. Stöcker, *Nucl. Phys. A* 476, 718 (1988)
- [14] O.V. Lozhkin and W. Trautmann, *Phys. Rev. C* 46, 1996 (1992)
- [15] G.J. Kunde, S. Gaff, C.K. Gelbke, T. Glasmacher, M.J. Huang, R. Lemmon, W.G. Lynch, L. Manduci, L. Martin, M.B. Tsang, W.A. Friedman, J. Dempsey, R.J. Charity, L.G. Sobotka, D.K. Agnihotri, B. Djerroud, W.U. Schröder, W. Skulski, and J. Töke, *Phys. Lett. B* 416, 56 (1998)
- [16] J.P. Bondorf, A.S. Botvina, A.S. Iljinov, I.N. Mishustin, and K. Sneppen, *Phys. Rep.* 257, 133 (1995)
- [17] A.S. Botvina, I.N. Mishustin, M. Begemann-Blaich, J. Hubele, G. Imme, I. Iori, P. Kreuzt, G.J. Kunde, W.D. Kunze, V. Lindenstruth, U. Lynen, A. Moroni, W.F.J. Müller, C.A. Ogilvie, J. Pochodzalla, G. Raciti, Th. Rubehn, H. Sann, A. Schüttauf, W. Seidel, W. Trautmann, and A. Wörner, *Nucl. Phys. A* 584, 737 (1995)
- [18] S.P. Avdeyev, V.A. Karnaukhov, W.D. Kuznetsov, L.A. Petrov, V.K. Rodionov, A.S. Zubkevich, H. Oeschler, O.V. Bochkarev, L.V. Chulkov, E.A. Kuzmin, A. Budzanovski, W. Karcz, M. Jan-

- icki, E. Norbeck, A.S. Botvina, W.A. Friedman, W. Nörenberg, and G. Papp, *Eur. Phys. J. A* 3, 75 (1998)
- [19] G. Wang, K. Kwiatkowski, D.S. Bracken, E. Renshaw Foxford, W.-c. Hsi, K.B. Morley, V.E. Viola, N.R. Yoder, C. Volant, R. Legrain, E.C. Pollacco, R.G. Korteling, W.A. Friedman, A. Botvina, J. Brzychczyk, and H. Breuer, *Phys. Rev. C* 60, 014603 (1999)
- [20] V.D. Toneev and K.K. Gudima, *Nucl. Phys. A* 400, 173c (1983)
- [21] A.S. Botvina, A.S. Iljinov, and I.N. Mishustin, *Nucl. Phys. A* 507, 649 (1990)
- [22] J.-J. Gaimard and K.-H. Schmidt, *Nucl. Phys. A* 531, 709 (1991)
- [23] J. Pochodzalla, T. Möhlenkamp, T. Rubehn, A. Schüttauf, A. Wörner, E. Zude, M. Begemann-Blaich, Th. Blaich, H. Emling, A. Ferrero, C. Groß, G. Immé, I. Iori, G.J. Kunde, W.D. Kunze, V. Lindenstruth, U. Lynen, A. Moroni, W.F.J. Müller, B. Ocker, G. Raciti, H. Sann, C. Schwarz, W. Seidel, V. Serfling, J. Stroth, W. Trautmann, A. Trzcinski, A. Tucholski, G. Verde, and B. Zwieglinski, *Phys. Rev. Lett.* 75, 1040 (1995)
- [24] A.S. Botvina and I.N. Mishustin, *Phys. Lett. B* 294, 23 (1992)
- [25] H.W. Barz, W. Bauer, J.P. Bondorf, A.S. Botvina, R. Donangelo, H. Schulz, and K. Sneppen, *Nucl. Phys. A* 561, 466 (1993)
- [26] Bao-An Li, A.R. DeAngelis, and D.H.E. Gross, *Phys. Lett. B* 303, 225 (1993)
- [27] A. Schüttauf, W.D. Kunze, A. Wörner, M. Begemann-Blaich, Th. Blaich, D.R. Bowman, R.J. Charity, A. Cosmo, A. Ferrero, C.K. Gelbke, C. Groß, W.C. Hsi, J. Hubele, G. Immé, I. Iori, J. Kempter, P. Kreuzer, G.J. Kunde, V. Lindenstruth, M.A. Lisa, W.G. Lynch, U. Lynen, M. Mang, T. Möhlenkamp, A. Moroni, W.F.J. Müller, M. Neumann, B. Ocker, C.A. Ogilvie, G.F. Peaslee, J. Pochodzalla, G. Raciti, F. Rosenberger, Th. Rubehn, H. Sann, C. Schwarz, W. Seidel, V. Serfling, L.G. Sobotka, J. Stroth, L. Stuttgé, S. Tomasevic, W. Trautmann, A. Trzcinski, M.B. Tsang, A. Tucholski, G. Verde, C.W. Williams, E. Zude, and B. Zwieglinski, *Nucl. Phys. A* 607, 457 (1996)
- [28] S. Albergo, S. Costa, E. Costanzo, and A. Rubbino, *Il Nuovo Cimento* 89 A, 1 (1985)
- [29] M.B. Tsang, W.G. Lynch, H. Xi, and W.A. Friedman, *Phys. Rev. Lett.* 78, 3836 (1997)
- [30] K. Kwiatkowski, A.S. Botvina, D.S. Bracken, E. Renshaw Foxford, W.A. Friedman, R.G. Korteling, K.B. Morley, E.C. Pollacco, V.E. Viola, and C. Volant, *Phys. Lett. B* 423, 21 (1998)
- [31] J.A. Hauger, B.K. Srivastava, S. Albergo, F. Bieser, F.P. Brady, Z. Caccia, D.A. Cebra, A.D. Chacon, J.L. Chance, Y. Choi, S. Costa, J.B. Elliott, M.L. Gilkes, A.S. Hirsch, E.L. Hjort, A. Insolia, M. Justice, D. Keane, J.C. Kintner, V. Lindenstruth, M.A. Lisa, H.S. Matis, M. McMahan, C. McParland, W.F.J. Müller, D.L. Olson, M.D. Partlan, N.T. Porile, R. Potenza, G. Rai, J. Rasmussen, H.G. Ritter, J. Romanski, J.L. Romero, G.V. Russo, H. Sann, R.P. Scharenberg, A. Scott, Y. Shao, T.J.M. Symons, M. Tincknell, C. Tuvé, S. Wang, P. Warren, H.H. Wieman, T. Wienold, and K. Wolf, *Phys. Rev. C* 62, 024616 (2000)
- [32] M. Veselsky, R.W. Ibbotson, R. Laforest, E. Ramakrishnan, D.J. Rowland, A. Ruangma, E.M. Winchester, E. Martin, and S.J. Yennello, *Phys. Lett. B* 497, 1 (2001)
- [33] A.S. Botvina, A.S. Iljinov, I.N. Mishustin, J.P. Bondorf, R. Donangelo, and K. Sneppen, *Nucl. Phys. A* 475, 663 (1987)
- [34] D.H.E. Gross, *Rep. Prog. Phys.* 53, 605 (1990)
- [35] D.H.E. Gross and K. Sneppen, *Nucl. Phys. A* 567, 317 (1994)
- [36] A.S. Botvina, A.S. Iljinov, and I.N. Mishustin, *Sov. J. Nucl. Phys.* 42, 712 (1985)
- [37] A.S. Botvina and I.N. Mishustin, *Phys. Rev. C* 63, 061601 (2001)
- [38] M.F. Rivet, Ch.O. Bacri, B. Borderie, J.D. Frankland, M. Assenard, G. Auger, F. Bocage, R. Bougault, R. Brou, Ph. Buchet, A. Chbihi, J. Colin, R. Dayras, A. Demeyer, D. Doré, D. Durand, P. Eudes, E. Galichet, E. Genouin-Duhamel, E. Gerlic, M. Germain, D. Guinet, P. Lantesse, J.L. Laville, J.F. Lecomte, A. Le Fèvre, T. Lefort, R. Legrain, N. Le Neindre, O. Lopez, M. Louvel, L. Nalpas, A.D. Nguyen, M. Parlog, J. Péter, E. Plagnol, A. Rahmani, T. Reposeur, E. Rosato, F. Saint-Laurent, S. Salou, M. Squalli, J.C. Steckmeyer, M. Stern, G. Tabacaru, B. Tamain, L. Tassan-Got, O. Tirel, D. Vintache, C. Volant, J.P. Wieleczko, A. Guarnera, M. Colonna, and P. Chomaz, *Phys. Lett. B* 430, 217 (1998)
- [39] M.D. Zubkov and O.V. Lozhkin, *Nucl. Phys. A* 626, 267c (1997)
- [40] N. Marie, A. Chbihi, J.B. Natowitz, A. Le Fèvre, S. Salou, J.P. Wieleczko, L. Gingras, M. Assenard, G. Auger, Ch.O. Bacri, F. Bocage, B. Borderie, R. Bougault, R. Brou, P. Buchet, J.L. Charvet, J. Cibor, J. Colin, D. Cussol, R. Dayras, A. Demeyer, D. Doré, D. Durand, P. Eudes, J.D. Frankland, E. Galichet, E. Genouin-Duhamel, E. Gerlic, M. Germain, D. Gourio, D. Guinet, K. Hagel, P. Lantesse, J.L. Laville, J.F. Lecomte, T. Lefort, R. Legrain, N. Le Neindre, O. Lopez, M. Louvel, Z. Majka, A.M. Maskay, L. Nalpas, A.D. Nguyen, M. Parlog, J. Péter, E. Plagnol, A. Rahmani, T. Reposeur, M.F. Rivet, E. Rosato, F. Saint-Laurent, J.C. Steckmeyer, M. Stern, G. Tabacaru, B. Tamain, O. Tirel, E. Vient, C. Volant, and R. Wada, *Phys. Rev. C* 58, 256 (1998)
- [41] L. Beaulieu, K. Kwiatkowski, W.-c. Hsi, T. Lefort, L. Pienkowski, R.G. Korteling, G. Wang, B. Back, D.S. Bracken, H. Breuer, E. Cornell, F. Gimeno-Nogues, D.S. Ginger, S. Gushue, M.J. Huang, R. Laforest, W.G. Lynch, E. Martin, K.B. Morley, L.P. Rensberg, D. Rowland, E. Ramakrishnan, A. Ruangma, M.B. Tsang, V.E. Viola, E. Winchester, H. Xi, and S.J. Yennello, *Phys. Lett. B* 463, 159 (1999)
- [42] L. Beaulieu, T. Lefort, K. Kwiatkowski, R.T. de Souza, W.-c. Hsi, L. Pienkowski, B. Back, D.S. Bracken, H. Breuer, E. Cornell, F. Gimeno-Nogues, D.S. Ginger, S. Gushue, R.G. Korteling, R. Laforest, E. Martin, K.B. Morley, E. Ramakrishnan, L.P. Rensberg, D. Rowland, A. Ruangma, V.E. Viola, G. Wang, E. Winchester, and S.J. Yennello, *Phys. Rev. Lett.* 84, 5971 (2000)